

Cell-Edge-Aware Precoding for Downlink Massive MIMO Cellular Networks

Howard H. Yang, *Student Member, IEEE*, Giovanni Geraci, *Member, IEEE*,
Tony Q. S. Quek, *Senior Member, IEEE*, and Jeffrey G. Andrews, *Fellow, IEEE*

Abstract—We propose a *cell-edge-aware* (CEA) zero forcing (ZF) precoder that exploits the excess spatial degrees of freedom provided by a large number of base station (BS) antennas to suppress inter-cell interference at the most vulnerable user equipments (UEs). We evaluate the downlink performance of CEA-ZF, as well as that of a conventional *cell-edge-unaware* (CEU) ZF precoder in a network with random base station topology. Our analysis and simulations show that the proposed CEA-ZF precoder outperforms CEU-ZF precoding in terms of (i) aggregate per-cell data rate, (ii) coverage probability, and (iii) 95%-likely, or edge user, rate. In particular, when both perfect channel state information and a large number of antennas N are available at the BSs, we demonstrate that the outage probability under CEA-ZF and CEU-ZF decay as $1/N^2$ and $1/N$, respectively. This result identifies CEA-ZF as a more effective precoding scheme for massive MIMO cellular networks. Our framework also reveals the importance of scheduling the optimal number of UEs per BS, and confirms the necessity to control the amount of pilot contamination received during the channel estimation phase.

Index Terms—Multi-user downlink, 5G, cellular networks, inter-cell interference, massive MIMO, zero forcing precoding.

I. INTRODUCTION

Supporting the ever increasing wireless throughput demand is the primary factor driving the industry and academia alike towards the fifth generation (5G) wireless systems. Not only will 5G cellular networks have to provide a large aggregate capacity, but more importantly, they will have to guarantee high worst-case rates for all user equipments (UEs), including those located at the cell edge, i.e., close to interfering base stations (BSs) [1]–[3]. New technologies are being introduced to improve the performance of cell-edge UEs from current levels. Equipping BSs with a large number of antennas, widely known as massive multiple-input multiple-output (MIMO), has emerged as one of the most promising solutions [4]–[6]. In this work, we propose to use some of the spatial dimensions available at massive MIMO BSs to significantly improve the data rate of UEs at the cell edge, as well as the overall network throughput. To this end, we design and analyze a linear transmission scheme, termed *cell-edge-aware* (CEA) zero forcing (ZF) precoder, that suppresses interference at the cell-edge UEs.

H. H. Yang and T. Q. S. Quek are with the Singapore University of Technology and Design, Singapore (e-mail: hao_yang@mymail.sutd.edu.sg, tonyquek@sutd.edu.sg).

G. Geraci is with Bell Laboratories Nokia, Dublin, Republic of Ireland (e-mail: giovanni.geraci@nokia.com).

J. G. Andrews is with the University of Texas at Austin, Austin TX, USA (email: jandrews@ece.utexas.edu).

A. Motivation and Related Work

A considerable amount of research has investigated the use of multi-cell joint signal processing for cell-edge performance improvement [7]–[9]. The common idea behind joint processing techniques is to organize BSs in clusters, where BSs lying in the same cluster share information on the data to be transmitted to all UEs in the cluster. Although this information allows BSs to coordinate their transmissions and jointly serve all UEs with an improved system throughput, it comes at the cost of heavy signaling overhead and backhaul latency, which defy the purpose of its implementation [10].

As the benefits of joint processing are often outweighed by the increased latency and overhead, a more practical alternative to increase the cell-edge throughput can be found in coordinated beamforming, or *precoding*, schemes [11]–[13]. Under coordinated precoding, each BS acquires additional channel state information (CSI) of UEs in neighboring cells, but no data information is shared between the various BSs. The additional CSI can then be exploited to control the crosstalk generated at UEs in other cells, e.g., by using multiple BS antennas to steer the crosstalk towards the nullspace of the neighboring UEs. This approach is especially attractive for massive MIMO BSs, due to the abundance of spatial dimensions provided by the large antenna arrays [14].

Recent attempts to design and analyze a coordinated precoder for massive MIMO cellular networks are made in [15], [16]. The current paper differs from and generalizes these two works in two key aspects:

- 1) *Design*: Unlike [15], [16], where each BS suppresses the interference at all edge UEs in all neighboring cells, we specifically target those neighboring UEs close to the BS coverage area. Therefore, our precoder employs fewer spatial dimensions to mitigate inter-cell interference, leaving more degrees of freedom to each BS to better multiplex its own associated UEs [17].
- 2) *Analysis*: While [15], [16] assume a symmetric hexagonal cellular network, we consider a network model with random topology. Hexagonal models can lead to substantial performance overestimation, as demonstrated in [18], [19], whereas our analysis accounts for the randomness of practical cellular deployments.

B. Approach and Summary of Results

In this paper, we model the massive MIMO BS deployment and the UE locations as independent Poisson point processes (PPPs), where each BS simultaneously serves multiple UEs

on each time-frequency resource block (RB). By introducing a second-order Voronoi tessellation, we define the cell neighborhood of each BS, and design a CEA-ZF precoder that controls the interference generated in the neighborhood. Using random matrix theory and stochastic geometry, we analyze the coverage and rate performance of CEA-ZF, as well as that of a conventional *cell-edge-unaware* (CEU) ZF precoder, in a general setting that accounts for the interference affecting both the channel estimation and data transmission phases. Our contributions can be summarized as follows.

- We propose a new precoder for the downlink of massive MIMO cellular networks, which we denote as the CEA-ZF precoder, where some spatial dimensions are used to suppress inter-cell interference at the cell-edge neighboring UEs, and the remaining degrees of freedom are used to multiplex UEs within the cell. Our precoder works in a distributed manner, and it boosts network coverage and rate performance compared to CEU-ZF precoding.
- We develop a general framework to analyze the signal-to-interference ratio (SIR) distribution and coverage of massive MIMO cellular networks for both the proposed CEA-ZF and the CEU-ZF precoder. Our analysis is tractable and captures the effects of multi-antenna transmission, spatial multiplexing, path loss and small-scale fading, network load and BS deployment density, imperfect channel estimation, and random network topology.
- Through our analysis, which is validated via simulation results, we show that the proposed CEA-ZF precoder outperforms conventional CEU-ZF in terms of aggregate per-cell data rate and coverage probability. Moreover, CEA-ZF guarantees a significantly larger 95%-likely rate, i.e., it improves the cell-edge rate. When perfect CSI and a large number of antennas, N , are available at the BSs, we find that the outage probabilities under CEA-ZF and CEU-ZF decay as $1/N^2$ and $1/N$, respectively, demonstrating that CEA-ZF is a more effective precoding scheme for massive MIMO cellular networks.
- We quantify the effect of imperfect CSI, and reveal the importance of controlling the amount of pilot contamination received during the channel estimation phase, e.g., through smart pilot allocation schemes. We also study the system performance as a function of the network load, showing that the aggregate per-cell rate is sensitive to the number of UEs spatially multiplexed on the same RB.

The remainder of the paper is organized as follows. We introduce the system model in Section II. In Section III, we analyze the SIR and network coverage under CEA-ZF and CEU-ZF precoding, also providing simulations that confirm the accuracy of our analysis. We show the numerical results in Section IV to quantify the benefits of CEA-ZF precoding and obtain design insights. We conclude the paper in Section V.

II. SYSTEM MODEL

In this section, we introduce the network topology and propagation model, the CSI available at the BS, the conventional CEU-ZF precoder, and the proposed CEA-ZF precoder. The main notations used throughout the paper are summarized in Table I.

TABLE I
NOTATION SUMMARY

Notation	Definition
$\Phi_b; \lambda$	PPP modeling the location of BSs; BS deployment density
$N; K$	Number of transmit antennas per BSs; number of scheduled UEs per BS
$P_t; \alpha$	BS transmit power; path loss exponent
$\mathcal{C}_i; \mathcal{C}_i^N$	First-order Voronoi cell for BS i ; cell neighborhood for BS i
$\mathcal{C}_i^E = \mathcal{C}_i \cup \mathcal{C}_i^N$	Extended cell for BS i
$r_{iik}; r_{\bar{i}ik}$	Distance between UE k in cell i and its serving BS i and second closest BS \bar{i} , respectively
$\mathbf{x}_{ijk} \sim \mathcal{CN}(0, \mathbf{I}_N)$	Small-scale fading between BS i and UE k in cell j
$\mathbf{w}_{u,ik}; \mathbf{w}_{a,ik}$	CEU-ZF and CEA-ZF precoding vector, respectively, at BS i for its UE k
$M; F$	Available number of pilots; pilot reuse factor
\mathcal{I}_p	Interference during training phase
$\mathcal{I}_u; \mathcal{I}_a$	Interference during data transmission phase for CEU-ZF and CEA-ZF, respectively
τ_{ijk}	Standard deviation of CSI error between BS i and UE k in cell j
$\gamma_{ik}; \theta$	SIR at UE k in cell i ; SIR decoding threshold
$P_c(\theta); \rho_{95}$	Coverage probability; 95%-likely rate

A. Network Topology

We consider the downlink of a cellular network that consists of randomly deployed BSs, whose location follows a homogeneous PPP Φ_b of spatial density λ in the Euclidean plane.¹ We assume that each BS transmits with power P_t and is equipped with a large number of antennas, N .² Single-antenna UEs are distributed as an independent homogeneous PPP with sufficient high density on the plane, such that each BS has at least K candidate UEs in its cell, i.e., within its coverage area, to transmit to. In light of its higher spectral efficiency, we consider spatial multiplexing at the BSs, where in each time-frequency RB each BS simultaneously serves the K UEs in its cell with $K \leq N$ [4].

We assume that UEs associate to the BS that provides the largest average received power. Due to the homogeneous nature of the network, this results in a distance-based association rule.³ The set of UE locations that are associated to BS i located at $\mathbf{z}_i \in \mathbb{R}^2$ are defined by a classical Voronoi tessellation on the plane, denoted by \mathcal{V}_i^1 and given by [24], [25]

$$\mathcal{V}_i^1 = \{\mathbf{z} \in \mathbb{R}^2 \mid \|\mathbf{z} - \mathbf{z}_i\| \leq \|\mathbf{z} - \mathbf{z}_k\|, \forall \mathbf{z}_k \in \Phi_b \setminus \{\mathbf{z}_i\}\}. \quad (1)$$

We note that the set \mathcal{V}_i^1 contains all locations for which BS i is the closest. Such a definition is identical to that of a traditional cell, thus we equivalently denote \mathcal{V}_i^1 as \mathcal{C}_i .

In this work, we design a CEA-ZF precoder that controls the interference generated by each BS at the neighboring UEs.

¹PPPs serve as a good model for the planned deployment of macro cell BSs, as verified by both empirical evidence [20] and theoretical analysis [21].

²We note that power control, which may result in different transmit powers at the BSs, could be used in addition to interference suppression to increase the performance of cell-edge UEs.

³Different association rules apply when transmit power or large-scale fading vary among BSs, resulting in a weighted Voronoi diagram [22], [23].

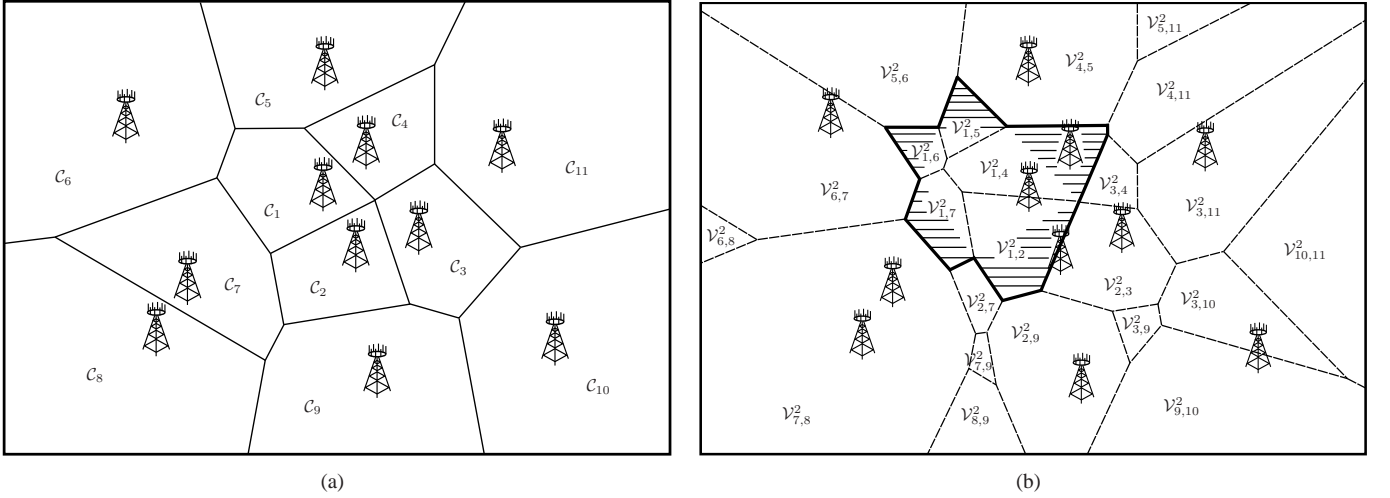


Fig. 1. Examples of (a) first-order and (b) second-order Voronoi tessellation. In (a), solid lines delimit first-order Voronoi cells C_i . In (b), dashed lines delimit second-order Voronoi cells $V_{i,j}^2$, solid lines delimit the extended cell C_1^E , and a shadowed region indicates the cell neighborhood C_1^N .

In order to identify the neighboring UEs for each BS, we find it useful to generalize the above definition of Voronoi cell to the second order. More precisely, the second-order Voronoi tessellation $V_{i,j}^2$ denotes the set of UE locations for which the BSs in \mathbf{z}_i and \mathbf{z}_j are the two closest, and it is given by [24], [25]

$$V_{i,j}^2 = \{ \mathbf{z} \in \mathbb{R}^2 \mid \cap_{l \in \{i,j\}} \{ \|\mathbf{z} - \mathbf{z}_l\| \leq \|\mathbf{z} - \mathbf{z}_k\| \} \mid \forall \mathbf{z}_k \in \Phi_b \setminus \{ \mathbf{z}_i, \mathbf{z}_j \} \}. \quad (2)$$

Using the second-order Voronoi tessellation, we can now define the notion of extended cell C_i^E for BS i , given by (i) all UEs for which BS i is the closest, and (ii) all UEs for which BS i is the second closest. The extended cell C_i^E is given by

$$C_i^E = \cup_j V_{i,j}^2, \quad \forall \mathbf{z}_j \in \Phi_b \setminus \mathbf{z}_i. \quad (3)$$

According to the above definition, each UE that lies in C_i^E sees BS i as either its closest or second closest BS. The extended cell C_i^E includes the UEs located in C_i that are served by BS i , as well as the neighboring UEs which are most vulnerable to interference generated by BS i . These UEs constitute the cell neighborhood for BS i , which we denote by C_i^N and define as follows

$$C_i^N = C_i^E \setminus C_i. \quad (4)$$

Fig. 1 illustrates the concepts of first-order and second-order Voronoi tessellation, cell neighborhood, and extended cell. Fig. 1(a) shows a realization of first-order Voronoi tessellation, where each BS i covers a cell C_i . Fig. 1(b) depicts the corresponding second-order Voronoi tessellation, where each pair of BSs (i, j) identifies a region $V_{i,j}^2$ (delimited by dashed lines), such that UEs located in $V_{i,j}^2$ have BS i and BS j as their closest and second closest, or vice versa. Fig. 1(b) also shows the extended cell C_1^E for BS 1 (delimited by solid lines), which is composed by the first-order cell C_1 and by the neighborhood C_1^N (shadowed region).

In this paper, we propose a CEA-ZF precoding scheme where each BS not only spatially multiplexes the associated UEs in C_i , but also suppresses the interference caused at the

most vulnerable neighboring UEs in C_i^N . We note that each BS i can easily obtain a list of UEs in C_i^N by means of reference signal received power (RSRP) estimation. In fact, downlink RSRP measurements for a list of neighboring BSs are periodically sent by each UE for handover purposes [26].

B. Channel Model and Estimation

In this network, we model the channels between any pair of antennas as independent and identically distributed (i.i.d.) and quasi-static, i.e., the channel is constant during a sufficiently long coherence block, and varies independently from block to block.⁴ Moreover, we assume that each channel is narrowband and affected by two attenuation components, namely small-scale Rayleigh fading, and large-scale path loss.⁵ As such, the channel matrix from BS i to its K associated UEs can be written as

$$\mathbf{H}_i = \mathbf{R}_i^{\frac{1}{2}} \mathbf{X}_i \quad (5)$$

where $\mathbf{R}_i = \text{diag}\{r_{i1}^{-\alpha}, \dots, r_{iK}^{-\alpha}\}$ is the path loss matrix, with r_{ijk} denoting the distance from the BS i to UE k in cell j , i.e., associated with BS j . The constant α represents the path loss exponent, whereas $\mathbf{X}_i = [\mathbf{x}_{i1}, \dots, \mathbf{x}_{iK}]^H$ is the $K \times N$ fading matrix, where $\mathbf{x}_{ijk} \sim \mathcal{CN}(0, \mathbf{I}_N)$ is the channel fading vector between BS i and UE k in cell j . Due to the interference-limited nature of massive MIMO cellular networks, we neglect the effect of thermal noise [4].

In order to simultaneously amplify the desired signal at the intended UEs and suppress interference at other UEs, each BS requires CSI from all the UEs it serves. This CSI is obtained during the training phase, where some RBs are used for the transmission of pilot signals. Since the number of pilots, i.e.,

⁴Note that the results obtained through the machinery of random matrix theory can be modified to model transmit antenna correlation [27]–[29].

⁵For the sake of tractability, the analysis presented here does not consider shadowing. Note that the results involving large-system approximations can be adjusted to account for the presence of shadowing as in [22]. Moreover, a generalized gamma approximation can still be used under shadowing, since the channel attenuation at a given UE follows a Rayleigh distribution [23].

the number of RBs allocated to the training phase, is limited, these pilots must be reused across cells. Pilot reuse implies that the estimate for the channel between a BS and one of its UEs is contaminated by the channels between the BS and UEs in other cells which share the same pilot [4]–[6], [30], [31].

Pilot contamination can be a limiting factor for the performance of massive MIMO. In order to mitigate this phenomenon, non-universal pilot reuse has been proposed, where neighboring cells use different sets of mutually orthogonal pilots [15], [19]. Under non-universal pilot reuse, the total set of available pilot sequences is divided into sub-groups, and different sub-groups are assigned to adjacent cells. For a pilot reuse factor F , the same sub-group of orthogonal pilot sequences is reused in every F cells.

We denote by $M = \kappa L$ the number of available orthogonal pilots, with L being the number of symbols that can be transmitted within a time-frequency coherence block, and κ being the fraction of symbols that are allocated for channel estimation. For a time-division duplexing (TDD) system with $L = 2 \times 10^4$ and $\kappa = 5\%$, there would be $M = 1000$ orthogonal pilots, and therefore a pilot reuse factor $F = 7$ would allow the estimation of 142 UE channels per cell [10].⁶ As a general rule, a pilot reuse factor $F \geq 3$ is recommended in order to mitigate pilot contamination [33]. In this regard, we assume that there are sufficient pilot sequences to support a large enough pilot reuse factor, such that each BS can estimate the CSI of UEs in its own cell and in adjacent cells.

In this paper, we express the estimated small-scale fading $\hat{\mathbf{x}}_{ijk}$ between BS i and UE k in cell j as

$$\hat{\mathbf{x}}_{ijk} = \sqrt{1 - \tau_{ijk}^2} \mathbf{x}_{ijk} + \tau_{ijk} \mathbf{q}_{ijk}, \quad (6)$$

where $\mathbf{q}_{ijk} \sim \mathcal{CN}(\mathbf{0}, \mathbf{I}_N)$ is an independent normalized estimation noise and τ_{ijk}^2 is the error variance [28], [34]–[37]. The parameter $\tau_{ijk}^2 \in [0, 1]$ reflects the accuracy of the estimated fading channel $\hat{\mathbf{x}}_{ijk}$, i.e., $\tau_{ijk}^2 = 0$ corresponds to perfect CSI while $\tau_{ijk}^2 = 1$ corresponds to no CSI at all. By applying MMSE as the channel estimation criterion, the CSI error variance at the typical UE can be written as [15], [17]

$$\begin{aligned} \tau_{ijk}^2 &= 1 - \frac{r_{ijk}^{-\alpha}}{\sum_{l \in \Phi_P} r_{ilk}^{-\alpha}} \\ &= \frac{1}{1 + \frac{r_{ijk}^{-\alpha}}{\sum_{l \in \Phi_P \setminus \{j\}} r_{ilk}^{-\alpha}}} \end{aligned} \quad (7)$$

where Φ_P indicates the set of BSs that have their UEs re-using the same pilot as UE k in cell j and are thus generating pilot contamination. As such, the estimated channel matrix at BS i can therefore be written as

$$\hat{\mathbf{H}}_i = \mathbf{R}_i^{\frac{1}{2}} \hat{\mathbf{X}}_i. \quad (8)$$

Despite its simplicity, the above CSI model allows us to investigate the impact of imperfect CSI on the performance of the proposed CEA-ZF precoder.

⁶In a TDD system, downlink channels can be estimated through uplink pilots thanks to channel reciprocity. This makes the training time proportional to the number of UEs. A frequency-division duplexing (FDD) system requires a considerably longer training time, proportional to the number of BS antennas, and is therefore less suitable for massive MIMO [4], [32].

C. Downlink Transmission

We now introduce two downlink transmission schemes: (i) the conventional CEU-ZF precoder and (ii) the proposed CEA-ZF precoder.

1) *Conventional CEU-ZF precoding*: With conventional zero forcing transmission, each BS i calculates its precoding matrix as [27], [38], [39]

$$\mathbf{W}_{u,i} = \frac{1}{\sqrt{\zeta_{u,i}}} \cdot \hat{\mathbf{H}}_i^H \left(\hat{\mathbf{H}}_i \hat{\mathbf{H}}_i^H \right)^{-1}, \quad (9)$$

where $\hat{\mathbf{H}}_i = [\hat{\mathbf{h}}_{ii1}, \dots, \hat{\mathbf{h}}_{iiK}]^H \in \mathbb{C}^{K \times N}$ is the estimated channel matrix, and $\zeta_{u,i}$ is a power normalization factor given by

$$\zeta_{u,i} = \text{tr} \left[\left(\hat{\mathbf{H}}_i \hat{\mathbf{H}}_i^H \right)^{-1} \right]. \quad (10)$$

The individual precoding vector from BS i to its UE k is the k^{th} column of the precoding matrix.

Note that ZF precoding has been shown to outperform maximum ratio transmission (MRT) in terms of per-cell sum-rate [15]. When the system dimensions make the ZF matrix inversion in (9) computationally expensive, a simpler truncated polynomial expansion can be employed with similar performance [40].

2) *Proposed CEA-ZF precoding*: Unlike CEU-ZF precoding, where all spatial dimensions available at each BS i are used to multiplex UEs within cell \mathcal{C}_i , the proposed CEA-ZF precoder exploits some spatial dimensions to suppress interference at the most vulnerable UEs, i.e., those lying in the BS's cell neighborhood \mathcal{C}_i^N . Such interference suppression is performed by all BSs in a distributed manner, and improves the cell-edge performance of the network, as well as the overall data rate and coverage. An illustration of the basic features of CEA-ZF is given in Fig. 2, where a multi-antenna BS spatially multiplexes its in-cell UEs while simultaneously suppressing interference at its neighboring UEs.

For BS i , we denote by K' the number of UEs lying in the cell neighborhood, where we omit the subscript i for notational convenience. We note that K' indicates the number of UEs for which BS i is the second closest, i.e., the number of neighboring UEs for BS i . The proposed CEA-ZF precoding matrix for BS i is then given by

$$\mathbf{W}_{a,i} = \frac{1}{\sqrt{\zeta_{a,i}}} \cdot \left\{ \hat{\mathbf{H}}_{i,E}^H \left(\hat{\mathbf{H}}_{i,E} \hat{\mathbf{H}}_{i,E}^H \right)^{-1} \right\}_{[1:K]}, \quad (11)$$

where $\hat{\mathbf{H}}_{i,E} = [\hat{\mathbf{h}}_{ii1}, \dots, \hat{\mathbf{h}}_{iiK}, \hat{\mathbf{h}}_{i\bar{i}1}, \dots, \hat{\mathbf{h}}_{i\bar{i}K'}]^H \in \mathbb{C}^{(K+K') \times N}$, with $\{\mathbf{H}\}_{[1:K]}$ indicating the first K columns of the matrix \mathbf{H} , and $\hat{\mathbf{h}}_{i\bar{i}l}$ denoting the estimated channel between BS i and the l -th neighboring UE, where the notation \bar{i} indicates that BS i is the second closest BS for that particular UE. The constant $\zeta_{a,i}$ is chosen as an average power normalization factor, given by

$$\zeta_{a,i} = \text{tr} \left[\left(\left\{ \hat{\mathbf{H}}_{i,E}^H \left(\hat{\mathbf{H}}_{i,E} \hat{\mathbf{H}}_{i,E}^H \right)^{-1} \right\}_{[1:K]} \right)^2 \right]. \quad (12)$$

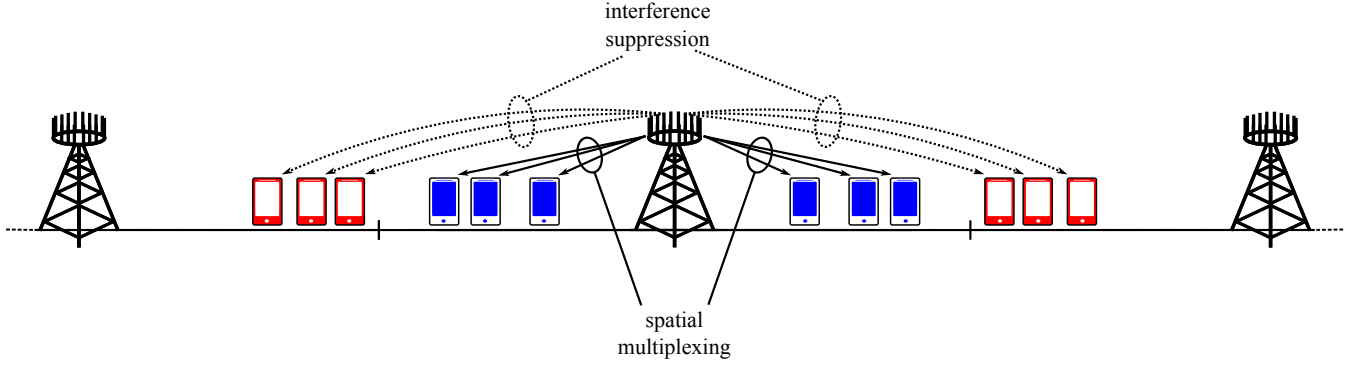


Fig. 2. Illustration of CEA-ZF where a BS performs spatial multiplexing for in-cell UEs and interference suppression for neighboring UEs.

We note that the CEA-ZF precoder in (11) can be seen as a generalization of the two-cell precoder proposed in [11] to a non-symmetric and non-pairwise scenario.

Remark 1: The pseudo inverse in (11) aims at projecting interference onto the null space spanned by the channels of all UEs in the extended cell \mathcal{C}_i^E . In other words, CEA-ZF sacrifices certain degrees of freedom to null the BS interference towards not only in-cell UEs but also out-cell edge UEs. As a result, edge UEs can enjoy lower inter-cell interference, at the expense of fewer degrees of freedom being available at the BSs to provide spatial multiplexing gain. A tradeoff therefore exists between the amount of interference to be suppressed and the remaining degrees of freedom for spatial multiplexing. In fact, the higher the number of out-cell UEs to which a BS suppresses interference, the smaller the number of spatial dimensions for multiplexing gain, and vice versa. Nevertheless, as long as the total number of degrees of freedom is larger than the total number of spatial dimensions needed for UE multiplexing and interference suppression, transmissions from a BS to the served UEs are guaranteed to be interference free under CEA-ZF.

III. COVERAGE ANALYSIS

In this section, we analyze the downlink SIR coverage of a massive MIMO cellular network with conventional CEU-ZF precoding and the proposed CEA-ZF precoding, and then provide simulations that verify the accuracy of our analysis.

A. Preliminaries

1) *SIR at a typical UE:* By applying Slivnyak's theorem to the stationary PPP of BSs, it is sufficient to evaluate the SIR of a typical UE at the origin [41]. In the following, we denote as *typical* the UE k associated with BS i , with a received signal given by

$$y_{ik} = P_t \mathbf{h}_{iik}^H \mathbf{w}_{ik} s_{ik} + \sum_{l=1, l \neq k}^K P_t \mathbf{h}_{iil}^H \mathbf{w}_{il} s_{il} + \sum_{j \neq i} \sum_{l=1}^K P_t \mathbf{h}_{jik}^H \mathbf{w}_{jl} s_{jl} \quad (13)$$

where $\mathbf{w}_{ik} \in \mathbb{C}^{N \times 1}$ is the normalized precoding vector from the serving BS i to the typical UE, and s_{ik} is the corresponding

unit-power signal, i.e., $\mathbb{E}[|s_{ik}|^2] = 1$. The vector \mathbf{w}_{ik} can take different forms, depending on the precoding scheme employed. The SIR at the typical UE can be written as

$$\gamma_{ik} = \frac{|\mathbf{h}_{iik}^H \mathbf{w}_{ik}|^2}{\sum_{l=1, l \neq k}^K |\mathbf{h}_{iil}^H \mathbf{w}_{il}|^2 + \mathcal{I}}, \quad (14)$$

where the first summation in the denominator represents the intra-cell interference, while \mathcal{I} denotes the aggregate out-of-cell interference. The latter is given by

$$\mathcal{I} = \sum_{j \neq i} \frac{g_{jik}}{r_{jik}^\alpha}, \quad (15)$$

where g_{jik} is the effective small-scale fading from interfering BS j to UE k in cell i , given by

$$g_{jik} = \sum_{l=1}^K |\mathbf{x}_{jik}^H \mathbf{w}_{jl}|^2. \quad (16)$$

We note that when the precoding vectors $\{\mathbf{w}_{jl}\}_{l=1}^K$ at BS j are mutually independent and satisfy $\sum_{l=1}^K \|\mathbf{w}_{jl}\|^2 = 1$, the effective channel fading is distributed as $g_{jik} \sim \Gamma(K, 1/K)$ [42].

2) *Coverage probability:* Since both the received signal strength and the interference at a given UE are governed by a number of stochastic processes, e.g., random spatial distribution of transmitting/receiving nodes and small-scale fading, the resulting SIR is a random variable. In our analysis, the performance metric of interest is the coverage probability, defined as the probability that the received SIR γ at a generic UE is above a given threshold θ , i.e.,

$$P_c(\theta) = \mathbb{P}(\gamma \geq \theta), \quad \theta > 0. \quad (17)$$

We note that the coverage probability $P_c(\theta)$ provides information on the UE SIR (and therefore achievable rate) distribution across the network.

3) *CSI error:* Under sufficient non-universal pilot reuse, a generic BS i can estimate the channels of all in-cell UEs as well as the channels of neighboring UEs. From (7), the CSI error variance for an in-cell UE and for a neighboring UE can

be respectively written as

$$\tau^2 = \frac{1}{1 + \frac{t^{-\alpha}}{\mathcal{I}_p}}, \quad (18)$$

$$\bar{\tau}^2 = \frac{1}{1 + \frac{s^{-\alpha}}{\mathcal{I}_p}} \quad (19)$$

where t and s denote the distance between a typical UE and its closest and second closest BS, respectively, and \mathcal{I}_p is the pilot interference received during the training phase.

Under reuse factor F , clusters of F adjacent cells choose different sub-groups of pilot sequences and do not cause interference, i.e., pilot contamination to each other. Therefore, each BS receives pilot contamination only from UEs lying outside the cluster of F cells, whose mean area can be calculated as F/λ [41]. This area can be approximated with a circle $B(0, R_e)$ of radius $R_e = \sqrt{F/(\lambda\pi)}$ [43], yielding the following mean interference via Campbell's theorem [41]

$$\begin{aligned} \mathbb{E}[\mathcal{I}_p] &= \mathbb{E} \left[\sum_{x \in \Phi_P \cap B^c(0, R_e)} \|x\|^{-\alpha} \right] \\ &= \frac{2(\lambda\pi/F)^{\frac{\alpha}{2}}}{\alpha - 2}, \end{aligned} \quad (20)$$

where $B^c(0, R_e)$ denotes the complement set of $B(0, R_e)$. By approximating the interference \mathcal{I}_p with its mean [9] and by substituting (20) into (18) and (19), the CSI error can be approximated by a function of t and s as follows:

$$\tau^2 \approx \frac{1}{1 + \frac{(\alpha-2)F^{\frac{\alpha}{2}}}{2(\lambda\pi)^{\frac{\alpha}{2}} t^\alpha}}, \quad (21)$$

$$\bar{\tau}^2 \approx \frac{1}{1 + \frac{(\alpha-2)F^{\frac{\alpha}{2}}}{2(\lambda\pi)^{\frac{\alpha}{2}} s^\alpha}}. \quad (22)$$

B. CEU-ZF Precoding

We now derive the coverage probability under CEU-ZF precoding. An approximation of the SIR under CEU-ZF can be obtained in the large-system regime as follows.

Lemma 1: *Conditioned on the out-of-cell interference \mathcal{I}_u and the intra-cell distance r_{iil} , $l \in \{1, \dots, K\}$, when $K, N \rightarrow \infty$ with fixed $\beta = K/N < 1$, the SIR achieved by CEU-ZF precoding converges almost surely to the following quantity*

$$\gamma_{u,ik} - \frac{(1 - \tau_{iik}^2)(1 - \beta)N}{(\tau_{iik}^2 r_{iik}^{-\alpha} + \mathcal{I}_u)(r_{iik}^\alpha + R_k)} \rightarrow 0 \quad (23)$$

where R_k is given by

$$R_k = \sum_{l=1, l \neq k}^K r_{iil}^\alpha. \quad (24)$$

Proof: See Appendix A. \square

The accuracy of Lemma 1 will be verified in Fig. 3.

Deriving the coverage probability requires knowledge of the distribution of R_k , which is the sum of $(K-1)$ i.i.d. random variables (r.v.s) r_{iil}^α . The distance r_{iil} is a r.v. that follows a Rayleigh distribution $f_c(r)$, given by [44]

$$f_c(r) = 2\pi\lambda r e^{-\lambda\pi r^2}. \quad (25)$$

It can then be shown that r_{iil}^α follows a Weibull distribution with shape and scale parameters $2/\alpha$ and $(\lambda\pi)^{-\frac{\alpha}{2}}$, respectively [45]. As such, the distribution of R_k can be approximated by a generalized Gamma distribution as follows [46].

Assumption 1: *The probability density function (pdf) $f_{R_k}(r)$ and cumulative density function (CDF) $F_{R_k}(r)$ of the r.v. R_k can be approximated as follows*

$$f_{R_k}(r) \approx \frac{\eta\mu^\eta r^{\eta\mu-1}}{\Omega^\mu \Gamma(\mu)} \exp\left(-\frac{\mu r^\eta}{\Omega}\right), \quad (26)$$

$$F_{R_k}(r) \approx \frac{1}{\Gamma(\mu)} \Gamma\left(\mu, \frac{\mu r^\eta}{\Omega}\right), \quad (27)$$

where $\Gamma(s, x) = \int_0^x t^{s-1} e^{-t} dt$ is the lower incomplete gamma function, and $\Omega = \mathbb{E}[R_k^\eta]$ is a scale parameter, given by

$$\Omega = \left[\frac{\mu^{\frac{1}{\eta}} \Gamma(\mu) \mathbb{E}[R_k]}{\Gamma\left(\mu + \frac{1}{\eta}\right)} \right]^\eta \quad (28)$$

while μ and η are solutions of the following equations

$$\frac{\Gamma^2\left(\mu + \frac{1}{\eta}\right)}{\Gamma(\mu) \Gamma\left(\mu + \frac{2}{\eta}\right) - \Gamma^2\left(\mu + \frac{1}{\eta}\right)} = \frac{\mathbb{E}[R_k]}{\mathbb{E}[R_k^2] - \mathbb{E}^2[R_k]}, \quad (29)$$

$$\frac{\Gamma^2\left(\mu + \frac{2}{\eta}\right)}{\Gamma(\mu) \Gamma\left(\mu + \frac{4}{\eta}\right) - \Gamma^2\left(\mu + \frac{2}{\eta}\right)} = \frac{\mathbb{E}[R_k^2]}{\mathbb{E}[R_k^4] - \mathbb{E}^2[R_k^2]}. \quad (30)$$

The quantities $\mathbb{E}[R_k]$, $\mathbb{E}[R_k^2]$, and $\mathbb{E}[R_k^4]$ are the first, second, and fourth moment of the r.v. R_k , respectively, and can be calculated as

$$\mathbb{E}[R_k] = \frac{K-1}{(\lambda\pi)^{\frac{\alpha}{2}}} \Gamma\left(1 + \frac{\alpha}{2}\right), \quad (31)$$

$$\mathbb{E}[R_k^2] = \frac{K-1}{(\lambda\pi)^\alpha} \left[\Gamma(1+\alpha) + (K-2) \Gamma^2\left(1 + \frac{\alpha}{2}\right) \right], \quad (32)$$

$$\begin{aligned} \mathbb{E}[R_k^4] &= \frac{K-1}{(\lambda\pi)^{2\alpha}} \left[(K-2)(K-3)(K-4) \Gamma^4\left(1 + \frac{\alpha}{2}\right) \right. \\ &\quad \left. + 3(K-2) \Gamma^2(1+\alpha) + 4(K-2) \Gamma\left(1 + \frac{\alpha}{2}\right) \Gamma\left(1 + \frac{3\alpha}{2}\right) \right. \\ &\quad \left. + \Gamma(1+2\alpha) + 6(K-2)(K-3) \Gamma(1+\alpha) \Gamma^2\left(1 + \frac{\alpha}{2}\right) \right]. \end{aligned} \quad (33)$$

The accuracy of the approximation in Assumption 1 will be verified in Fig. 4.

By using the approximated distribution of R_k , we can now obtain the coverage probability of a massive MIMO cellular network under CEU-ZF.

Theorem 1: *The coverage probability of a massive MIMO cellular network under CEU-ZF precoding can be approximated as*

$$\begin{aligned} \mathbb{P}(\gamma_{u,ik} \geq \theta) &\approx \frac{1}{\Gamma(\mu)} \int_0^\infty \Gamma\left(\mu, \frac{\mu}{\Omega} \left[\frac{(1-\tau^2)(1-\beta)Nr^\alpha}{\theta\left(\tau^2 + \frac{2\pi\lambda r^2}{\alpha-2}\right)} - r^\alpha \right]^\eta\right) f_c(r) dr \end{aligned} \quad (34)$$

where τ^2 is given in (21), and $f_c(r)$ is given by (25).

Proof: See Appendix B. \square

We note that although coverage probability of a multi-user MIMO cellular network with conventional CEU-ZF precoding has also been derived in [42], [47], [48], the result in (34) provides an approximation that involves only one integration and is therefore easier to be evaluated. The accuracy of this approximation will be verified in Fig. 5.

C. CEA-ZF Precoding

We now derive the coverage probability under the proposed CEA-ZF precoder. An approximation of the SIR under CEA-ZF can be obtained in the large-system regime as follows.

Lemma 2: *Conditioned on the out-of-cell interference \mathcal{I}_a , the intra-cell distance r_{il} with $l \in \{1, \dots, K\}$, the distance r_{iik} between the typical UE and its second closest BS, and the standard deviation τ_{iik} of the corresponding CSI error, when $K, N \rightarrow \infty$ with fixed $\beta = K/N < 1$ and fixed $\beta' = K'/N < 1$, the SIR of CEA-ZF converges almost surely to a quantity given by*

$$\gamma_{a,ki} - \frac{(1 - \tau_{iik}^2)(1 - \beta - \beta')N}{(\tau_{iik}^2 r_{iik}^{-\alpha} + \tau_{iik}^2 r_{iik}^{-\alpha} + \mathcal{I}_a)(r_{iik}^\alpha + R_k)} \rightarrow 0. \quad (35)$$

Proof: See Appendix C. \square

The accuracy of Lemma 2 will be verified in Fig. 3.

Using the above results, we are now able to derive the coverage probability under CEA-ZF precoding.

Theorem 2: *The coverage probability of a massive MIMO cellular network under CEA-ZF can be approximated as*

$$\begin{aligned} & \mathbb{P}(\gamma_{a,ik} \geq \theta) \\ & \approx \int_0^\infty \int_t^\infty \mathbb{E}_{K'} \left[\Gamma \left(\mu, \frac{\mu}{\Omega} \left[\frac{(1-\tau^2)(1-\beta-\beta')Ns^\alpha}{\theta(\bar{\tau}^2 + \tau^2 \frac{s^\alpha}{t^\alpha} + \frac{2\pi\lambda s^2}{\alpha-2})} - t^\alpha \right] \right)^\eta \right] \\ & \quad \times \frac{f_{s|c}(s, t)f_c(t)}{\Gamma(\mu)} ds dt \end{aligned} \quad (36)$$

where τ^2 and $\bar{\tau}^2$ are given in (21) and (22), respectively, and

$$f_{s|c}(s, t) = 2\pi\lambda s e^{-\lambda\pi(s^2-t^2)}. \quad (37)$$

Proof: See Appendix D. \square

The result in (36) involves an expectation on the number K' of neighboring UEs. While the number K of UEs associated to each BS is constant and depends on the scheduling process, K' is a r.v. whose distribution is generally unknown. In the following, we provide a more compact approximation for the coverage probability under CEA-ZF by approximating K' with its mean value, derived as follows.

Proposition 1: *The expected number of neighboring UEs for each BS, K' , satisfies*

$$\mathbb{E}[K'] = K. \quad (38)$$

Proof: See Appendix E. \square

Corollary 1: *By replacing K' with its mean K , the coverage probability of a massive MIMO cellular network under*

CEA-ZF can be further approximated as

$$\begin{aligned} & \mathbb{P}(\gamma_{a,ik} \geq \theta) \\ & \approx \int_0^\infty \int_t^\infty \Gamma \left(\mu, \frac{\mu}{\Omega} \left[\frac{(1-\tau^2)(1-2\beta)Ns^\alpha}{\theta(\bar{\tau}^2 + \tau^2 \frac{s^\alpha}{t^\alpha} + \frac{2\pi\lambda s^2}{\alpha-2})} - t^\alpha \right]^\eta \right) \\ & \quad \times \frac{f_{s|c}(s, t)f_c(t)}{\Gamma(\mu)} ds dt. \end{aligned} \quad (39)$$

Proof: The result follows from (36) by approximating $\beta' = K'/N$ with its mean value $\beta = K/N$. \square

The accuracy of Corollary 1 will be verified in Fig. 6.

D. Asymptotic Results

Equations (34) and (39) quantify how some of the key features of a cellular network, i.e., deployment strategy, interference, and impairments in the channel estimation phase, affect the coverage probability under CEA-ZF and CEU-ZF precoding. Based on these results, simple asymptotic expressions for the coverage probability can be obtained when perfect CSI is assumed available at the massive MIMO BSs.

Corollary 2: *Under perfect CSI, i.e., $\tau = \bar{\tau} = 0$, when $\alpha = 4$ and $\beta = \frac{K}{N} \ll 1$, the network coverage probabilities under CEU-ZF and CEA-ZF can be respectively approximated by the following quantities*

$$\mathbb{P}(\gamma_{u,ik} \geq \theta) \approx 1 - 2\beta\theta = 1 - \frac{2K\theta}{N}, \quad (40)$$

$$\mathbb{P}(\gamma_{a,ik} \geq \theta) \approx 1 - (2\beta\theta)^2 = 1 - \frac{4K^2\theta^2}{N^2}. \quad (41)$$

Proof: See Appendix F. \square

The two following observations can be readily made from (41) and (42).

Observation 1: *In the asymptotic regime, CEA-ZF achieves higher coverage probability than CEU-ZF only when $\beta < \frac{1}{2\theta}$, or equivalently, $N > 2\theta K$. This observation indicates that CEA-ZF requires a sufficiently large number of BS antennas to attain good performance.*

Observation 2: *For a large number of antennas, N , the outage probabilities under CEA-ZF, $1 - \mathbb{P}(\gamma_{a,ik} \geq \theta)$, and under CEU-ZF, $1 - \mathbb{P}(\gamma_{u,ik} \geq \theta)$, decay as $\frac{1}{N^2}$ and $\frac{1}{N}$, respectively. These scaling laws prove CEA-ZF more effective for coverage enhancement in massive MIMO cellular networks.*

We note that although the approximations (40) and (41) only hold asymptotically, a similar behavior can be observed under imperfect CSI and for a finite number of BS antennas, as we will show in Section IV.

E. Analysis Validation

We now show simulation results that confirm the accuracy of our analytical framework. Unless differently specified, we use the following parameters for path loss exponent, BS density, and number of UE, respectively: $\alpha = 4$, $\lambda = 10^{-6}\text{m}^{-2} = 1/\text{km}^2$, and $K = 10$.

In Fig. 3, we depict the downlink SIR achieved by a typical UE of a massive MIMO cellular network as a function of the number of BS antennas N , under different precoding

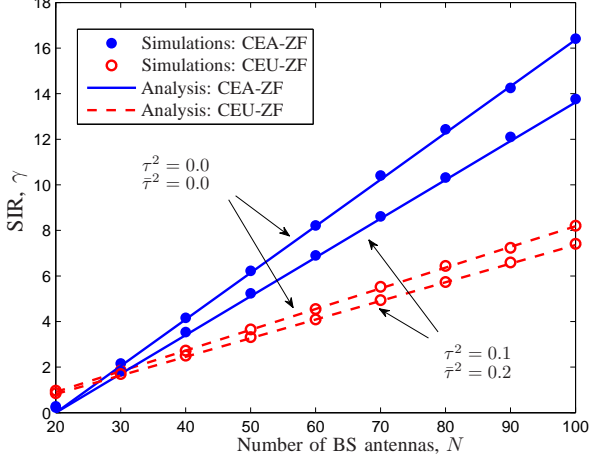


Fig. 3. Downlink SIR for CEU-ZF and CEA-ZF versus number of BS antennas, for scenarios with and without CSI error.

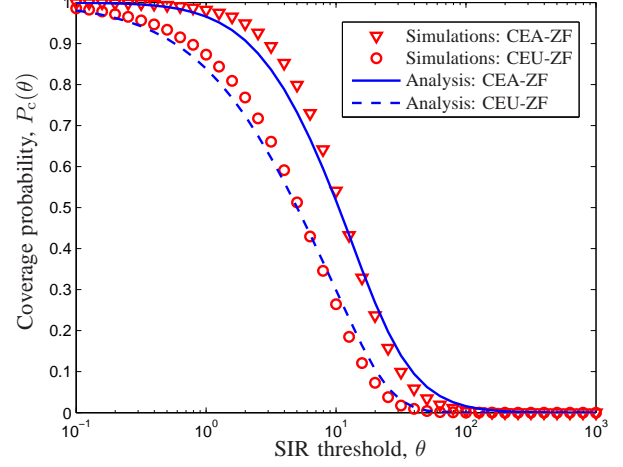


Fig. 5. Coverage probability under CEU-ZF and CEA-ZF precoding: analysis versus simulations.

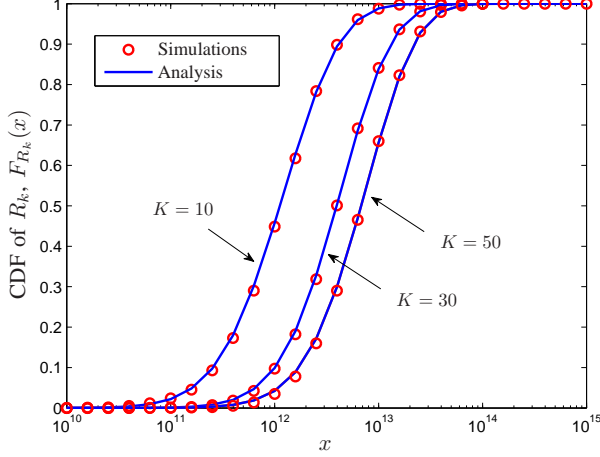


Fig. 4. CDF of the r.v. R_k in (24) and proposed approximation in Assumption 1, for BS density $\lambda = 10^{-6}$ and different numbers of UE per cell, K .

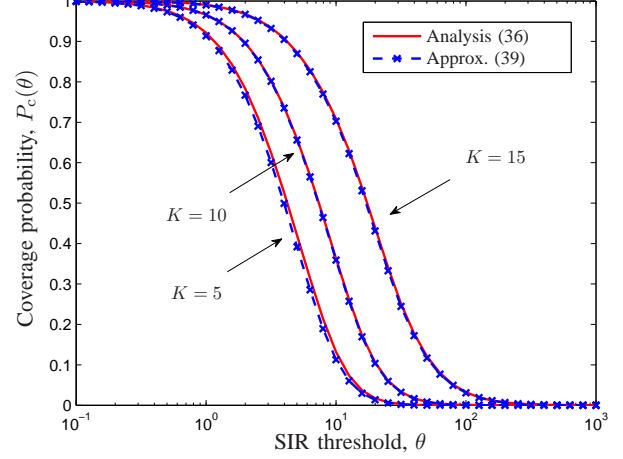


Fig. 6. Coverage probability under CEA-ZF precoding (Theorem 2) and its approximation (Corollary 1).

schemes and transmit CSI errors. The figure shows a negligible difference between simulations and analytical results, which confirms the accuracy of Lemma 1 and Lemma 2. We also note that the SIR values obtained for ZF precoding are consistent with the ones obtained in [17].

In Fig. 4, we compare the simulated CDF of the r.v. R_k in (24) to the generalized gamma approximation proposed in Assumption 1, for various values of the number of scheduled UE per cell, K . The figure shows a close match for all values of K , which confirms the accuracy of Assumption 1.

Fig. 5 compares the simulated coverage probability to the analytical results derived in Theorem 1 and Theorem 2. The coverage probability is plotted versus the SIR threshold at the typical UE. The figure shows that analytical results and simulations fairly well match and follow the same trend, thus confirming the accuracy of the theorems.

Fig. 6 compares the coverage probability derived analyti-

cally in Theorem 2 and its approximation in Corollary 1. It can be seen that the two results match well under different values of K , hence confirming the accuracy of Corollary 1.

IV. NUMERICAL RESULTS AND DISCUSSION

In this section, we provide numerical results to show the performance gain attained by the proposed CEA-ZF precoder, and we discuss how data rate and coverage are affected by the number of scheduled UEs and the channel estimation accuracy.

A. Numerical Results

Unless otherwise stated, the following system parameters will be used: BS deployment density $\lambda = 10^{-6} \text{m}^{-2}$, i.e., $\lambda = 1 \text{BS/km}^2$, number of scheduled UEs per cell $K = 20$, path loss exponent $\alpha = 3.8$, and pilot reuse factor $F = 7$. In this paper, the data rate for an SIR γ is calculated as $\mathcal{R} = K\mathbb{E}[\log_2(1 + \gamma)]$, and it does not account for the

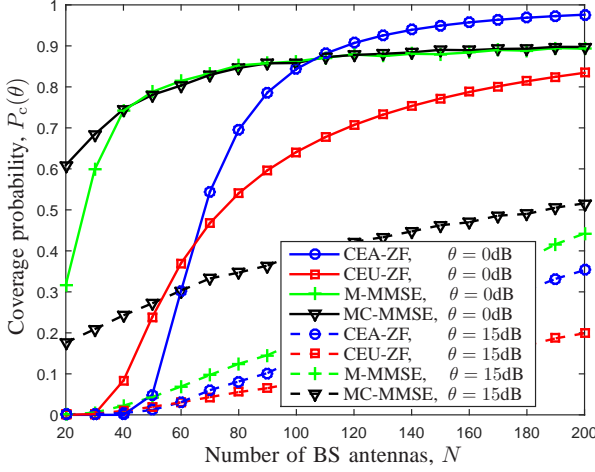


Fig. 7. Coverage probability versus number of BS antennas for $K = 20$ scheduled UEs per cell, under M-MMSE, MC-MMSE, CEU-ZF, and CEA-ZF precoding.

fraction of time spent for training, since this depends on the pilot allocation scheme employed. We note that neglecting the training time does not affect the fairness of our performance comparison between different precoding schemes. In the following, the performance of the proposed CEA-ZF precoder is compared to the one of CEU-ZF, as well as to two multi-cell MMSE precoders, i.e., the M-MMSE precoder [49] and the MC-MMSE precoder [50].

Fig. 7 depicts the coverage probability under M-MMSE, MC-MMSE, CEU-ZF, and CEA-ZF precoding as a function of the number of BS antennas N , for two different SIR thresholds θ . The following can be observed: (i) a switching point exists, i.e., CEA-ZF outperforms CEU-ZF precoding only if the number of BS antennas exceeds a certain value, (ii) as the number of BS antennas grows, the coverage probability under CEA-ZF converges to one faster than that under CEU-ZF, and (iii) CEA-ZF attains the best coverage probability when the SIR threshold is low, while MC-MMSE and M-MMSE outperform CEA-ZF in high-SIR regime. We note that observations (i) and (ii) are consistent with the ones we made in Section III-D in an asymptotic regime with perfect CSI, and observation (iii) comes from the fact that both M-MMSE and MC-MMSE have an intrinsic regularization factor to balance between signal gain and interference, whereas CEA-ZF is dedicated to suppress strong interference at the cell edge and thus is more suitable for low-SIR scenarios.

In Fig. 8, we compare the 95%-likely rate under the four precoding schemes. The 95%-likely rate (denoted by ρ_{95}) is defined as the rate achievable by at least 95% of the UEs in the network, and it can be regarded as the worst rate any scheduled UE may expect to receive when located at the cell edge [3], [4]. While the 95%-likely rates of both CEU-ZF and CEA-ZF precoding benefit from a larger number of BS antennas N , the proposed CEA-ZF precoder achieves a significantly larger 95%-likely rate compared to conventional CEU-ZF, and the gain increases as N grows. We note that M-MMSE and MC-

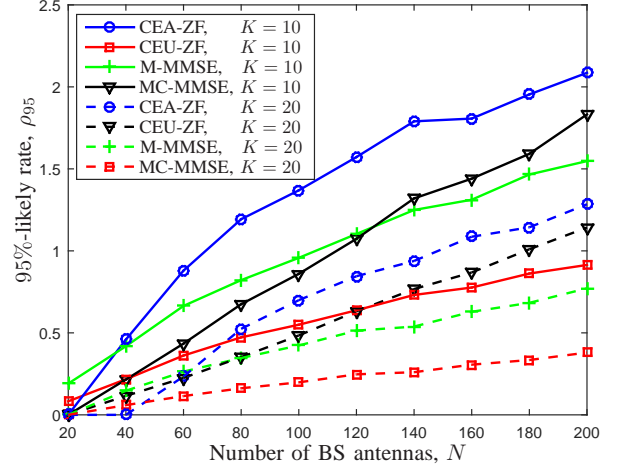


Fig. 8. 95%-likely rate versus number of BS antennas, with M-MMSE, MC-MMSE, CEU-ZF, and CEA-ZF precoding

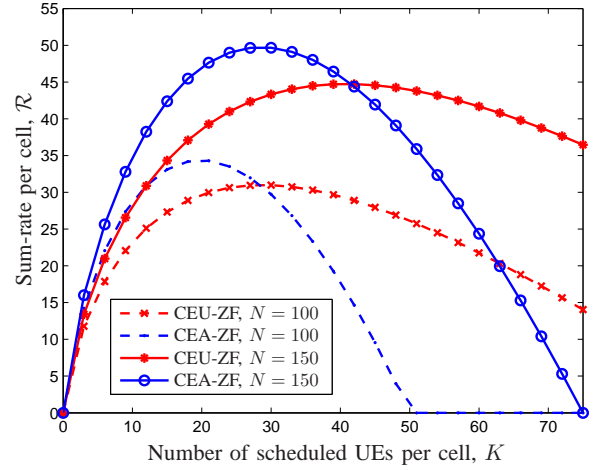


Fig. 9. Sum ergodic rate versus number of UEs per cell, for different numbers of BS antennas, N .

MMSE can also provide improved 95%-likely rates over CEU-ZF, as both of them implicitly suppress interference towards cell-edge UEs by balancing between signal gain and interference. Nevertheless, CEA-ZF achieves the best performance in terms of 95%-likely rate, because it employs fewer spatial dimensions to mitigate inter-cell interference, leaving more degrees of freedom for multiplexing gain.

Fig. 9 compares the sum-rate per cell under CEU-ZF and CEA-ZF as a function of the number of scheduled UEs per cell, K . An optimal value of K that maximizes the sum-rate exists for both CEU-ZF and CEA-ZF precoding, due to a tradeoff between simultaneously serving more UEs and having fewer spatial dimensions available for interference suppression. Fewer UEs should be scheduled under CEA-ZF, thus leaving more spatial dimensions for cell-edge interference suppression, and achieving a higher sum-rate compared to conventional CEU-ZF precoding.

We now study the impact of the channel estimation er-

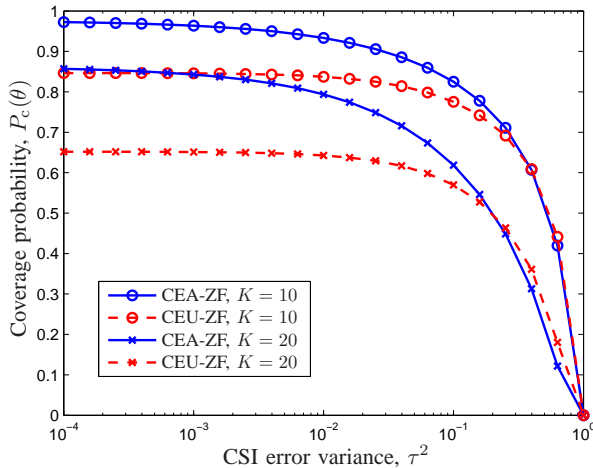


Fig. 10. Coverage probability plotted as a function of CSI error variance.

error on coverage and edge rates. To this end, we vary the CSI error variance τ^2 and $\bar{\tau}^2$ at in-cell UEs and neighboring UEs, respectively, while keeping their ratio constant as $\mathbb{E}[\bar{\tau}^2]/\mathbb{E}[\tau^2] = 1.8$. In the following we set the SIR threshold as $\theta = 0$ dB and number of BS antennas as $N = 100$.

Fig. 10 shows the coverage probability as a function of the CSI error for various values of scheduled UEs per cell. Although the presence of a CSI error degrades the coverage probability of both CEU-ZF and CEA-ZF precoding, it can be seen that CEA-ZF significantly outperforms conventional CEU-ZF for low-to-moderate values of the CSI error. Under a large CSI error, CEA-ZF still performs as well as CEU-ZF as long as the number of scheduled UEs per cell is controlled, e.g., $K = 10$ or $K = 20$ in the figure.

Fig. 11 depicts the 95%-likely rate as a function of the CSI error variance for CEU-ZF and CEA-ZF precoding. Once again, CEA-ZF significantly outperforms conventional CEU-ZF for low-to-moderate values of the CSI error, while the 95%-likely rates of both precoders degrade and achieve similar values under very poor CSI quality, i.e., large values of τ^2 and $\bar{\tau}^2$.

B. Discussion

The main takeaways provided by our analytical framework are outlined as follows.

1) *Performance gain*: The proposed CEA-ZF precoder outperforms conventional CEU-ZF precoding from several perspectives. CEA-ZF provides better coverage than CEU-ZF, especially in the massive MIMO regime, i.e., when BSs are equipped with a large number of antennas, N . While CEA-ZF can attain high coverage probability with reasonable values of N , a significantly larger number of antennas is required to achieve the same coverage under CEU-ZF precoding. The proposed CEA-ZF precoder also achieves a larger sum-rate per cell, and a significantly larger 95%-likely rate. The latter is especially important, being the worst data rate that any scheduled UE can expect to receive.

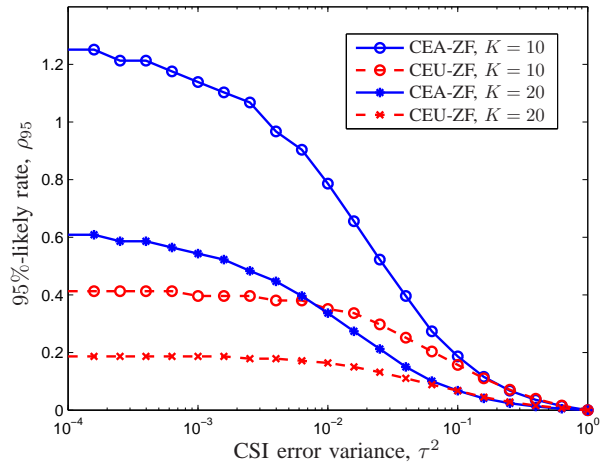


Fig. 11. 95%-likely rate plotted as a function of CSI error variance.

2) *UE scheduling*: The aggregate sum-rate per cell is sensitive to the number of UEs K simultaneously served through spatial multiplexing, for both CEU-ZF and CEA-ZF precoding. It is therefore important to schedule the right number of UEs for transmission as a function of the number of BS antennas, N . The proposed CEA-ZF precoder is slightly more sensitive to variations of K . The rationale behind such phenomenon is that when N just merely exceeds K , sacrificing extra spatial dimensions to suppress interference at neighboring UEs cannot compensate for the loss in power gain experienced by the in-cell UEs. On the other hand, when $K \ll N$, not enough UEs are being multiplexed, and some of the available degrees of freedom are being “wasted” in power gain, while they could instead yield higher multiplexing gain [33]. We note that multiplexing gain enhances the rate linearly, whereas power gain only enhances the rate logarithmically, i.e., at a lower pace.

3) *Channel estimation error*: As expected, pilot contamination can negatively affect the achievable data rates by degrading the quality of the CSI available at the BSs. In the presence of very large channel estimation errors, the performance of CEA-ZF precoding degrades and converges to the one of conventional CEU-ZF precoding. In fact, the cell-edge suppression mechanism employed by CEA-ZF relies on the accuracy of the measured channels, and the promised gains in terms of coverage and 95%-likely rate cannot be achieved. It is therefore desirable to control the amount of pilot contamination received during the channel estimation phase, for example by designing appropriate pilot allocation schemes.

V. CONCLUSIONS

In this paper, we proposed the CEA-ZF precoder, which exploits the excess spatial degrees of freedom available at massive MIMO BSs to suppress inter-cell interference at the most vulnerable UEs in the network. Unlike joint processing techniques, CEA-ZF can be implemented in a distributed fashion. Moreover, CEA-ZF specifically targets those neighboring UEs close to the BS coverage area, thus requiring fewer spatial

dimensions to mitigate inter-cell interference, and leaving more dimensions for intra-cell spatial multiplexing.

In order to model practical deployments, we analyzed the performance of CEA-ZF and conventional CEU-ZF precoding in a random asymmetric cellular network. We showed that a higher per-cell data rate and a better network coverage can be guaranteed by the CEA-ZF precoder. More importantly, the 95%-likely rate, namely the minimum data rate that any UE can expect to achieve, is significantly improved. The latter is of particular interest, given the ambitious edge rate requirements set for 5G, which aims for an uninterrupted high data rate user experience. While this paper focused on the downlink of cellular networks, CEA-ZF can also be employed as an uplink receive filter to remove the interference generated by UEs in nearby cells. Similar gains are expected in the uplink setting, although this should be verified in future work. Besides, the proposed CEA-ZF could be combined with suitable power control schemes to further enhance the cell-edge rates. Additionally, this work modeled the BS deployment with a PPP, which may tend to overestimate the cell edge effects. Evaluating the gains in a more realistic scenario, e.g., by introducing a minimum BS inter-site distance, is also left as future work.

Our study also quantified the impact of imperfect CSI, confirming the importance of controlling the amount of pilot contamination during the channel estimation phase. While our emphasis was on the SIR distribution across the network, the data rate may also be affected by the amount of resources dedicated to pilot signals. An inherent tradeoff exists between mitigating pilot contamination and reusing pilot resources. To this end, fractional pilot reuse (FPR) has been proposed in [16], [51], where cell-center UEs of neighboring cells reuse the same pilots, while cell-edge UEs employ non-universal pilot reuse. Analyzing the performance of FPR in randomly deployed networks is regarded as an interesting research direction.

APPENDIX

A. Proof of Lemma 1

Conditioned on the out of cell interference \mathcal{I}_u , we substitute the expression of $\mathbf{w}_{u,ik}$ in (9) into (14), then as $K, N \rightarrow \infty$ with $\beta = K/N < 1$, the SIR γ converges to the following [27, Theorem 14.3]

$$\gamma_{u,ik} - \frac{1 - \tau_{iik}^2}{\Upsilon \cdot r_{iik}^{-\alpha} \tau_{iik}^2 + \Psi \cdot \mathcal{I}_u} \rightarrow 0, \text{ a.s.} \quad (42)$$

where Υ and Ψ are given by

$$\Upsilon = \frac{1}{\phi} \frac{1}{N} \text{tr} \mathbf{R}_i^{-1}, \quad (43)$$

$$\Psi = \frac{\psi}{\frac{N}{K} \phi^2 - \psi} \frac{1}{K} \frac{1}{N} \text{tr} \mathbf{R}_i^{-1} \quad (44)$$

and ψ and ϕ are given, respectively, by

$$\psi = \frac{1}{N} \text{tr} \left(\mathbf{I}_N + \frac{K}{N} \frac{1}{\phi} \mathbf{I}_N \right)^{-2} = \frac{1}{\left(1 + \frac{\beta}{\phi}\right)^2}, \quad (45)$$

$$\phi = \frac{1}{N} \text{tr} \left[\left(1 + \frac{\beta}{\phi}\right) \mathbf{I}_N \right]^{-1} = \frac{1}{1 + \frac{\beta}{\phi}}. \quad (46)$$

By solving (45) and (46), we obtain $\phi = 1 - \beta$ and $\psi = \phi^2$. By substituting ψ and ϕ in (43) and (44), respectively, the following holds

$$\Upsilon = \Psi = \frac{1}{N} \frac{1}{1 - \beta} \sum_{l=1}^K r_{iil}^\alpha. \quad (47)$$

Lemma 1 then follows by substituting (47) into (42).

B. Proof of Theorem 1

Consider a typical UE k in cell i and located at the origin. We denote the distance between the typical UE and its serving BS i as $r_{iik} = t$. As such, we can approximate the out of cell interference \mathcal{I}_u by its mean, which can be computed as

$$\begin{aligned} \mathbb{E}[\mathcal{I}_u] &= \mathbb{E} \left[\sum_{x \in \Phi_b \setminus i} \frac{g_{xik}}{\|x\|^\alpha} \right] \\ &\stackrel{(a)}{=} \int_t^\infty r^{-\alpha} r dr = \frac{2\pi\lambda t^{-(\alpha-2)}}{\alpha-2} \end{aligned} \quad (48)$$

where (a) is obtained by taking expectation of the effective fading g_{xik} and then using Campbell's theorem [41, Theorem 1.4.3]. By substituting (48) into (23), the conditional SIR received at the typical UE can be approximated as

$$\gamma_{u,ik} \approx \frac{(1 - \tau_{iik}^2)(1 - \beta)N}{\left(\tau_{iik}^2 t^{-\alpha} + \frac{2\pi\lambda t^{-(\alpha-2)}}{\alpha-2}\right)(t^\alpha + R_k)}. \quad (49)$$

The coverage probability can then be calculated as

$$\begin{aligned} &\mathbb{P}(\gamma_{u,ik} \geq \theta) \\ &\approx \mathbb{E} \left[\mathbb{P} \left(R_k \leq \frac{(1 - \tau_{iik}^2)(1 - \beta)N t^\alpha}{\left(\tau_{iik}^2 + \frac{2\pi\lambda t^2}{\alpha-2}\right)\theta} - t^\alpha \middle| r_{iik} = t \right) \right]. \end{aligned} \quad (50)$$

Since the pdf of t has been given in (25), Theorem 1 then follows from (50) by deconditioning t .

C. Proof of Lemma 2

We start with the minimum-mean-square-error (MMSE) version of the CEA-ZF precoder, which includes a regularization term $\rho \mathbf{I}_N$, given by

$$\tilde{\mathbf{w}}_{a,ik} = \frac{1}{\sqrt{\hat{\zeta}_{a,i}}} \left(\rho N \mathbf{I}_N + \sum_{l=1}^K \hat{\mathbf{h}}_{iil} \hat{\mathbf{h}}_{iil}^H + \sum_{l=1}^{K'} \hat{\mathbf{h}}_{iil} \hat{\mathbf{h}}_{iil}^H \right)^{-1} \hat{\mathbf{h}}_{iik} \quad (51)$$

where $\tilde{\zeta}_{a,i}$ satisfies that $\sum_{k=1}^K \|\tilde{\mathbf{w}}_{a,ik}\|^2 = 1$. The SIR at the typical UE can be written as

$$\gamma_{a,ik} = \frac{|\mathbf{h}_{iik}^H \tilde{\mathbf{w}}_{a,ik}|^2}{\sum_{l \neq k} |\mathbf{h}_{iik}^H \tilde{\mathbf{w}}_{a,il}|^2 + \sum_{l=1}^K |\mathbf{h}_{iik}^H \tilde{\mathbf{w}}_{a,il}|^2 + I_a}. \quad (52)$$

Substituting (8) into the numerator of (52), and using the matrix inversion lemma and the rank-1 permutation lemma [27, Theorem 3.9], the received signal power converges to the following limit in the large-system regime

$$|\mathbf{h}_{iik}^H \tilde{\mathbf{w}}_{a,ik}|^2 - \frac{(1 - \tau_{iik}^2)}{\tilde{\zeta}_{a,i}} \frac{(r_{iik}^{-\alpha} \Lambda_i)^2}{(1 + r_{iik}^{-\alpha} \Lambda_i)^2} \rightarrow 0, \quad \text{as } N \rightarrow \infty \quad (53)$$

where Λ_i is the solution of the following fix point equation [52, Theorem 13]

$$\Lambda_i = \frac{1}{\rho + \frac{1}{N} \sum_{l=1}^K \frac{r_{iil}^{-\alpha}}{1 + \Lambda_i r_{iil}^{-\alpha}} + \frac{1}{N} \sum_{l=1}^{K'} \frac{r_{iil}^{-\alpha}}{1 + \Lambda_i r_{iil}^{-\alpha}}}. \quad (54)$$

We next deal with the first two summations in the denominator of (52), which are the intra-cell interference from the serving BS and the inter-cell interference from the second closest interfering BS. Similarly, by using the rank-1 permutation again, the large-system limit for these interference reads as

$$\begin{aligned} & \sum_{l \neq k} |\mathbf{h}_{iik}^H \tilde{\mathbf{w}}_{a,il}|^2 \\ &= \sum_l \frac{\frac{1}{\tilde{\zeta}_{a,i}} \frac{r_{iil}^{-\alpha}}{N} \left(-\frac{\partial \Lambda_i}{\partial \rho} \right)}{(1 + r_{iil}^{-\alpha} \Lambda_i)^2} \left[\frac{(1 - \tau_{iik}^2) r_{iik}^{-\alpha}}{(1 + r_{iik}^{-\alpha} \Lambda_i)^2} + \tau_{iik}^2 r_{iik}^{-\alpha} \right], \end{aligned} \quad (55)$$

and

$$\begin{aligned} & \sum_l |\mathbf{h}_{iik}^H \tilde{\mathbf{w}}_{a,il}|^2 \\ &= \sum_l \frac{\frac{1}{\tilde{\zeta}_{a,i}} \frac{r_{iil}^{-\alpha}}{N} \left(-\frac{\partial \Lambda_i}{\partial \rho} \right)}{(1 + r_{iil}^{-\alpha} \Lambda_i)^2} \left[\frac{(1 - \tau_{iik}^2) r_{iik}^{-\alpha}}{(1 + r_{iik}^{-\alpha} \Lambda_i)^2} + \tau_{iik}^2 r_{iik}^{-\alpha} \right], \end{aligned} \quad (56)$$

respectively. For the power normalization factor $\tilde{\zeta}_{a,i}$ and $\tilde{\zeta}_{a,\bar{i}}$, the deterministic equivalence under large-system regime can be derived in a similar way as

$$\tilde{\zeta}_{a,i} \rightarrow \frac{1}{N} \sum_{l=1}^K \frac{r_{iil}^{-\alpha} \left(-\frac{\partial \Lambda_i}{\partial \rho} \right)}{(1 + r_{iil}^{-\alpha} \Lambda_i)^2}, \quad \tilde{\zeta}_{a,\bar{i}} \rightarrow \frac{1}{N} \sum_{l=1}^K \frac{r_{iil}^{-\alpha} \left(-\frac{\partial \Lambda_{\bar{i}}}{\partial \rho} \right)}{(1 + r_{iil}^{-\alpha} \Lambda_{\bar{i}})^2}. \quad (57)$$

As such, we have the deterministic equivalence of SIR being

$$\gamma_{a,ik} = \frac{(1 - \tau_{iik}^2) \frac{(r_{iik}^{-\alpha} \Lambda_i)^2}{(1 + r_{iik}^{-\alpha} \Lambda_i)^2} \left| \frac{1}{N} \sum_{l=1}^K \frac{r_{iil}^{-\alpha} \left(-\frac{\partial \Lambda_i}{\partial \rho} \right)}{(1 + r_{iil}^{-\alpha} \Lambda_i)^2} \right|^{-1}}{\frac{(1 - \tau_{iik}^2) r_{iik}^{-\alpha}}{(1 + r_{iik}^{-\alpha} \Lambda_i)^2} + \tau_{iik}^2 r_{iik}^{-\alpha} + \frac{(1 - \tau_{iik}^2) r_{iik}^{-\alpha}}{(1 + r_{iik}^{-\alpha} \Lambda_i)^2} + \tau_{iik}^2 r_{iik}^{-\alpha} + I_a}. \quad (58)$$

Finally, by letting $\rho \rightarrow 0$, each term in (58) that contains Λ_i respectively converges to

$$\frac{(r_{iik}^{-\alpha} \Lambda_i)^2}{(1 + r_{iik}^{-\alpha} \Lambda_i)^2} = \frac{(r_{iik}^{-\alpha} \rho \Lambda_i)^2}{(\rho + r_{iik}^{-\alpha} \rho \Lambda_i)^2} \rightarrow 1, \quad (59)$$

$$\frac{(1 - \tau_{iik}^2) r_{iik}^{-\alpha}}{(1 + r_{iik}^{-\alpha} \Lambda_i)^2} = \frac{(1 - \tau_{iik}^2) \rho^2 r_{iik}^{-\alpha}}{(\rho + \rho r_{iik}^{-\alpha} \Lambda_i)^2} \rightarrow 0, \quad (60)$$

$$\left| \frac{1}{N} \sum_{l=1}^K \frac{r_{iil}^{-\alpha} \left(-\frac{\partial \Lambda_i}{\partial \rho} \right)}{(1 + r_{iil}^{-\alpha} \Lambda_i)^2} \right|^{-1} \rightarrow \frac{(1 - \beta - \beta') N}{\sum_{l=1}^K r_{iil}^{-\alpha}}. \quad (61)$$

Lemma 2 then follows by substituting (59), (60), and (61) into (58).

D. Proof of Theorem 2

We consider a typical UE k of BS i that locates at the origin, and denote the distance between the UE and its associated BS as $r_{iik} = t$ and the distance from the UE to its second closest BS as $r_{iik} = s$. As such, we can approximate the out of cell interference \mathcal{I}_a by its mean based on Campbell's theorem [41], given as follows

$$\mathbb{E}[\mathcal{I}_a] = \mathbb{E} \left[\sum_{x \in \Phi_b \setminus \{i, \bar{i}\}} \frac{g_{xik}}{\|x\|^\alpha} \right] = \frac{2\pi \lambda s^{-(\alpha-2)}}{\alpha - 2}. \quad (62)$$

By substituting (62) into (35), the conditional SIR received at the typical UE can be approximated as

$$\gamma_{a,ik} \approx \frac{(1 - \tau_{iik}^2)(1 - \beta - \beta')N}{\left(\tau_{iik}^2 t^{-\alpha} + \tau_{iik}^2 s^{-\alpha} + \frac{2\pi \lambda s^{-(\alpha-2)}}{\alpha-2} \right) (t^\alpha + R_k)}. \quad (63)$$

The coverage probability can then be approximated as

$$\begin{aligned} & \mathbb{P}(\gamma_{a,ik} \geq \theta) \\ & \approx \mathbb{P} \left(R_k \leq \frac{(1 - \tau_{iik}^2)(1 - \beta - \beta')N\theta^{-1}}{\tau_{iik}^2 t^{-\alpha} + \tau_{iik}^2 s^{-\alpha} + \frac{2\pi \lambda s^{-(\alpha-2)}}{\alpha-2}} - t^\alpha \right). \end{aligned} \quad (64)$$

Theorem 2 then follows from (64) by deconditioning on t and s , with their pdf given in (25) and (37), respectively.

E. Proof of Proposition 1

Since the second-order Voronoi cells form a tessellation on \mathbb{R}^2 [41], the cell centers form a stationary point process Φ'_b with density λ' . Without loss of generality, we consider the center of the second-order Voronoi cell $\mathcal{V}_{x,y}^2$ as a typical point in Φ'_b located at the origin. We further denote the two BSs x and y that identify $\mathcal{V}_{x,y}^2$ as out-neighbors for the typical point 0. In this sense, under Palm probability \mathbf{P}^{00} , the set of out-neighbors for the origin 0 is formally defined as

$$h^+(\omega) = \{y \in \Phi_b : 0 \in \mathcal{V}_{y,z}^2, \quad z \in \Phi_b \setminus \{y\}\}. \quad (65)$$

By leveraging compatibility, we can define the out-neighbors of any point $X \in \Phi'_b$ as follows

$$H^+(X) = X + h^+(T_X) \quad (66)$$

where T_X is the shift operator defined in [53].

On the other hand, if BS x in Φ_b is regarded as typical, we can define in-neighbors for this typical point to be centers of all the second-order Voronoi cells constructed by BS x . Specifically, under Palm probability \mathbf{P}^0 , the set of in-neighbors for the origin 0 and any $Y \in \Phi_b$ can be respectively defined as

$$h^-(\omega) = \{y \in \Phi'_b : \mathcal{V}_{0,y}^2 \subseteq \mathcal{C}_0^E, \quad y \in \Phi'_b\}, \quad (67)$$

$$H^-(Y) = Y + h^-(T_Y). \quad (68)$$

Using the notations above, we are able to characterize the relationship between λ' and λ by the mass transport formula [41, Theorem 4.3.1]

$$\lambda' \mathbb{E}^{0'} [\text{card}(H^+(0))] = \lambda \mathbb{E}^0 [\text{card}(H^-(0))] \quad (69)$$

where $\text{card}(\cdot)$ is the cardinality of point's set of neighbors. Since $2\text{card}(H^+(0)) = \text{card}(H^-(0))$, it is $\lambda' = 2\lambda$. As such, if we denote \mathcal{V} as a typical Voronoi cell of Φ_b and \mathcal{V}' as a typical Voronoi cell of Φ'_b , the following holds by using the mass transport theorem [41]

$$\lambda \mathbb{E}^{0'} [|V \circ H^-(0)|] = \lambda' \mathbb{E}^0 [|V' \circ H^+(0)|] \quad (70)$$

where $|\cdot|$ denotes the Lebesgue measure and \circ denotes the composition operation. The above can be equivalently read as

$$\mathbb{E} [|\mathcal{C}_i^E|] = 2\mathbb{E} [|\mathcal{C}_i|]. \quad (71)$$

As a result, the expectation of K' can be calculated as

$$\mathbb{E} [K'] \stackrel{(a)}{=} \lambda_u \mathbb{E} [|\mathcal{C}_i^E|] - \lambda_u \mathbb{E} [|\mathcal{C}_i|] = K \quad (72)$$

where (a) follows from the fact that mean number of UEs in area \mathcal{A} is given by $\lambda_u |\mathcal{A}|$.

F. Proof of Corollary 2

We start with the asymptotic result for the network coverage probability under CEU-ZF. When $\tau^2 = 0$, $\bar{\tau}^2 = 0$, and $\alpha = 4$, using Fubini's theorem [45, Theorem 18.3], the coverage probability in (34) can be written as

$$\begin{aligned} \mathbb{P}(\gamma_{u,ik} \geq \theta) &\approx \frac{1}{\Gamma(\mu)} \int_0^\infty \exp\left(-\left(\frac{\Omega t}{\mu}\right)^{\frac{1}{\eta}} \frac{\pi(\lambda\pi)^2\theta}{(1-\beta)N}\right) t^{\mu-1} e^{-t} dt. \end{aligned} \quad (73)$$

As $\beta \ll 1$, the exponential term in (73) can be approximated by its first order Taylor expansion, as follows

$$\exp\left(-\frac{\pi(\lambda\pi)^2\theta(\Omega t/\mu)^{\frac{1}{\eta}}}{(1-\beta)N}\right) \approx 1 - \frac{\pi(\lambda\pi)^2\theta(\Omega t/\mu)^{\frac{1}{\eta}}}{(1-\beta)N}. \quad (74)$$

By substituting (74) into (73), the coverage probability under CEU-ZF reads as

$$\mathbb{P}(\gamma_{u,ik} \geq \theta) \approx 1 - \frac{\Gamma\left(\frac{1}{\eta} + \mu\right)}{\Gamma(\mu)} \left(\frac{\Omega}{\mu} t\right)^{\frac{1}{\eta}} \frac{(\lambda\pi)^2\theta}{(1-\beta)N}, \quad (75)$$

and (40) follows from using (28) and (31) into (75).

Similarly, using Fubini's theorem [45], we are able to approximate the coverage probability in (36) as follows

$$\begin{aligned} \mathbb{P}(\gamma_{a,ik} \geq \theta) &\approx \frac{1}{\Gamma(\mu)} \int_0^\infty \left(1 + \frac{(\Omega t/\mu)^{\frac{1}{\eta}} (\lambda\pi)^2\theta}{(1-2\beta)N}\right) \\ &\times \exp\left(-\frac{(\Omega t/\mu)^{\frac{1}{\eta}} (\lambda\pi)^2\theta}{(1-2\beta)N}\right) t^{\mu-1} e^{-t} dt. \end{aligned} \quad (76)$$

For $\beta \ll 1$, we have

$$\exp\left(-\frac{(\Omega t/\mu)^{\frac{1}{\eta}} (\lambda\pi)^2\theta}{(1-2\beta)N}\right) \approx 1 - \frac{(\Omega t/\mu)^{\frac{1}{\eta}} (\lambda\pi)^2\theta}{(1-2\beta)N}. \quad (77)$$

By substituting (77) into (76), the coverage probability under CEA-ZF reads as

$$\mathbb{P}(\gamma_{a,ik} \geq \theta) \approx 1 - \frac{\Gamma\left(\frac{2}{\eta} + \mu\right)}{\Gamma(\mu)} \left(\frac{\Omega}{\mu} t\right)^{\frac{2}{\eta}} \frac{(\lambda\pi)^4\theta^2}{(1-2\beta)^2 N^2}, \quad (78)$$

and (41) follows from using (28) and (32) into (78).

REFERENCES

- [1] Ericsson, "5G radio access - Capabilities and technologies," *white paper*, Apr. 2016.
- [2] Nokia Networks, "Ten key rules of 5G deployment - Enabling 1 Tbit/s/km² in 2030," *white paper*, Apr. 2015.
- [3] J. G. Andrews, S. Buzzi, W. Choi, S. V. Hanly, A. Lozano, A. C. Soong, and J. C. Zhang, "What will 5G be?" *IEEE J. Sel. Areas Commun.*, vol. 32, no. 6, pp. 1065–1082, Jun. 2014.
- [4] T. L. Marzetta, "Noncooperative cellular wireless with unlimited numbers of base station antennas," *IEEE Trans. Wireless Commun.*, vol. 9, no. 11, pp. 3590–3600, Nov. 2010.
- [5] F. Rusek, D. Persson, B. K. Lau, E. G. Larsson, T. L. Marzetta, O. Edfors, and F. Tufvesson, "Scaling up MIMO: Opportunities and challenges with very large arrays," *IEEE Signal Process. Mag.*, vol. 30, no. 1, pp. 40–60, Oct. 2013.
- [6] L. Lu, G. Y. Li, A. L. Swindlehurst, A. Ashikhmin, and R. Zhang, "An overview of massive MIMO: Benefits and challenges," *IEEE J. Sel. Topics Signal Process.*, vol. 8, no. 5, pp. 742–758, Oct. 2014.
- [7] G. Nigam, P. Minero, and M. Haenggi, "Coordinated multipoint joint transmission in heterogeneous networks," *IEEE Trans. Commun.*, vol. 62, no. 11, pp. 4134–4146, Nov. 2014.
- [8] Z. Xu, C. Yang, G. Y. Li, Y. Liu, and S. Xu, "Energy-efficient CoMP precoding in heterogeneous networks," *IEEE Trans. Signal Process.*, vol. 62, no. 4, pp. 1005–1017, Feb. 2014.
- [9] R. Tanbourgi, S. Singh, J. G. Andrews, and F. K. Jondral, "A tractable model for noncoherent joint-transmission base station cooperation," *IEEE Trans. Wireless Commun.*, vol. 13, no. 9, pp. 4959–4973, Sep. 2014.
- [10] A. Lozano, R. W. Heath Jr., and J. G. Andrews, "Fundamental limits of cooperation," *IEEE Trans. Inf. Theory*, vol. 59, no. 9, pp. 5213–5226, Sep. 2013.
- [11] R. Zakhour and S. V. Hanly, "Base station cooperation on the downlink: Large system analysis," *IEEE Trans. Inf. Theory*, vol. 58, no. 4, pp. 2079–2106, Apr. 2012.
- [12] R. Bhagavatula and R. W. Heath Jr., "Adaptive limited feedback for sum-rate maximizing beamforming in cooperative multicell systems," *IEEE Trans. Signal Process.*, vol. 59, no. 2, pp. 800–811, Jan. 2011.
- [13] Y. Huang, S. Durrani, and X. Zhou, "Interference suppression using generalized inverse precoder for downlink heterogeneous networks," *IEEE Wireless Commun. Lett.*, vol. 4, no. 3, pp. 325–328, Jun. 2015.
- [14] J. Hoydis, K. Hosseini, S. ten Brink, and M. Debbah, "Making smart use of excess antennas: Massive MIMO, small cells, and TDD," *Bell Labs Tech. J.*, vol. 18, no. 2, pp. 5–21, Sep. 2013.
- [15] E. Björnson, E. G. Larsson, and M. Debbah, "Massive MIMO for maximal spectral efficiency: How many users and pilots should be allocated?" *IEEE Trans. Wireless Commun.*, vol. 15, no. 2, pp. 1293–1308, Feb. 2016.

- [16] X. Zhu, Z. Wang, C. Qian, L. Dai, J. Chen, S. Chen, and L. Hanzo, "Soft pilot reuse and multi-cell block diagonalization precoding for massive MIMO systems," *IEEE Trans. Veh. Technol.*, vol. PP, no. 99, pp. 1–1, 2015.
- [17] J. Hoydis, S. ten Brink, and M. Debbah, "Massive MIMO in the UL/DL of cellular networks: How many antennas do we need?" *IEEE J. Sel. Areas Commun.*, vol. 31, no. 2, pp. 160–171, Feb. 2013.
- [18] Fujitsu Network Communications, "Enhancing LTE cell-edge performance via PDCCH ICIC," *white paper*, Mar. 2011.
- [19] E. Björnson and E. G. Larsson, "Three practical aspects of massive MIMO: Intermittent user activity, pilot synchronism, and asymmetric deployment," in *Proc. IEEE Global Telecomm. Conf.*, San Diego, CA, Dec. 2015, pp. 1–6.
- [20] D. B. Taylor, H. S. Dhillon, T. D. Novlan, and J. G. Andrews, "Pairwise interaction processes for modeling cellular network topology," in *Proc. IEEE Global Telecomm. Conf.*, Anaheim, CA, Dec. 2012, pp. 4524–4529.
- [21] B. Blaszczyzyn, M. K. Karray, and H. P. Keeler, "Using Poisson processes to model lattice cellular networks," in *Proc. IEEE Conf. on Computer Commun.* IEEE, Apr. 2013, pp. 773–781.
- [22] H. H. Yang, G. Geraci, and T. Q. S. Quek, "Energy-efficient design of MIMO heterogeneous networks with wireless backhaul," *IEEE Trans. Wireless Commun.*, vol. 5, no. 7, pp. 4914–4927, Jul. 2016.
- [23] S. Singh, X. Zhang, and J. G. Andrews, "Joint rate and SINR coverage analysis for decoupled uplink-downlink biased cell associations in HetNets," *IEEE Trans. Wireless Commun.*, vol. 14, no. 10, pp. 5360–5373, Oct. 2015.
- [24] D.-T. Lee, "On k-nearest neighbor Voronoi diagrams in the plane," *IEEE Trans. Comput.*, vol. 31, no. 6, pp. 478–487, Jun. 1982.
- [25] F. Baccelli and A. Giovanidis, "A stochastic geometry framework for analyzing pairwise-cooperative cellular networks," *IEEE Trans. Wireless Commun.*, vol. 14, no. 2, pp. 794–808, Feb. 2015.
- [26] D. Lopez-Perez, I. Guvenc, and X. Chu, "Mobility management challenges in 3GPP heterogeneous networks," *IEEE Commun. Mag.*, vol. 50, no. 12, pp. 70–78, Dec. 2012.
- [27] R. Couillet and M. Debbah, *Random matrix methods for wireless communications*. Cambridge University Press, 2011.
- [28] S. Wagner, R. Couillet, M. Debbah, and D. T. Stock, "Large system analysis of linear precoding in correlated MISO broadcast channels under limited feedback," *IEEE Trans. Inf. Theory*, vol. 58, no. 7, pp. 4509–4537, Mar. 2012.
- [29] G. Geraci, A. Y. Al-nahari, J. Yuan, and I. B. Collings, "Linear precoding for broadcast channels with confidential messages under transmit-side channel correlation," *IEEE Commun. Lett.*, vol. 17, no. 6, pp. 1164–1167, May 2013.
- [30] R. R. Müller, L. Cottatellucci, and M. Vehkaperä, "Blind pilot decontamination," *IEEE J. Sel. Topics Signal Process.*, vol. 8, no. 5, pp. 773–786, 2014.
- [31] G. C. Ferrante, G. Geraci, T. Q. S. Quek, and M. Z. Win, "Group-blind detection for uplink of massive MIMO systems," *IEEE Trans. Signal Process.*, 2016, to appear.
- [32] T. L. Marzetta and B. M. Hochwald, "Fast transfer of channel state information in wireless systems," *IEEE Trans. Signal Process.*, vol. 54, no. 4, pp. 1268–1278, Apr. 2006.
- [33] E. Björnson, E. G. Larsson, and T. L. Marzetta, "Massive MIMO: Ten myths and one critical question," *IEEE Commun. Mag.*, vol. 54, no. 2, pp. 114–123, Feb. 2016.
- [34] A. Müller, R. Couillet, E. Björnson, S. Wagner, and M. Debbah, "Interference-Aware RZF precoding for multicell downlink systems," *IEEE Trans. Signal Process.*, vol. 63, no. 15, pp. 3959–3973, Apr. 2015.
- [35] G. Geraci, R. Couillet, J. Yuan, M. Debbah, and I. B. Collings, "Large system analysis of linear precoding in MISO broadcast channels with confidential messages," *IEEE J. Sel. Areas Commun.*, vol. 31, no. 9, pp. 1660–1671, Aug. 2013.
- [36] B. Nosrat-Makouei, J. G. Andrews, and R. W. Heath, "MIMO interference alignment over correlated channels with imperfect CSI," *IEEE Trans. Signal Process.*, vol. 59, no. 6, pp. 2783–2794, Jun. 2011.
- [37] C. Wang and R. D. Murch, "Adaptive downlink multi-user mimo wireless systems for correlated channels with imperfect CSI," *IEEE Trans. Wireless Commun.*, vol. 5, no. 9, pp. 2435–2446, Sep. 2006.
- [38] G. Geraci, M. Egan, J. Yuan, A. Razi, and I. B. Collings, "Secrecy sum-rates for multi-user MIMO regularized channel inversion precoding," *IEEE Trans. Commun.*, vol. 60, no. 11, pp. 3472–3482, Nov. 2012.
- [39] C. B. Peel, B. M. Hochwald, and A. L. Swindlehurst, "A vector-perturbation technique for near-capacity multiantenna multiuser communication-part I: channel inversion and regularization," *IEEE Trans. Commun.*, vol. 53, no. 1, pp. 195–202, Feb. 2005.
- [40] A. Kammoun, A. Müller, E. Björnson, and M. Debbah, "Linear precoding based on polynomial expansion: Large-scale multi-cell MIMO systems," *IEEE J. Sel. Topics Signal Process.*, vol. 8, no. 5, pp. 861–875, Jan. 2014.
- [41] F. Baccelli and B. Blaszczyzyn, *Stochastic Geometry and Wireless Networks. Volume I: Theory*. Now Publishers, 2009.
- [42] G. Geraci, H. S. Dhillon, J. G. Andrews, J. Yuan, and I. B. Collings, "Physical layer security in downlink multi-antenna cellular networks," *IEEE Trans. Commun.*, vol. 62, no. 6, pp. 2006–2021, Jun. 2014.
- [43] R. W. Heath Jr., M. Kountouris, and T. Bai, "Modeling heterogeneous network interference using Poisson point processes," *IEEE Trans. Signal Process.*, vol. 61, no. 16, pp. 4114–4126, Aug. 2013.
- [44] M. Haenggi, *Stochastic geometry for wireless networks*. Cambridge University Press, 2012.
- [45] P. Billingsley, *Probability and measure*. John Wiley & Sons, 2008.
- [46] J. C. S. Santos Filho and M. D. Yacoub, "Simple precise approximations to Weibull sums," *IEEE Commun. Lett.*, vol. 10, no. 8, pp. 614–616, Aug. 2006.
- [47] H. S. Dhillon, M. Kountouris, and J. G. Andrews, "Downlink MIMO hetnets: Modeling, ordering results and performance analysis," *IEEE Trans. Wireless Commun.*, vol. 12, no. 10, pp. 5208–5222, Oct. 2013.
- [48] C. Li, J. Zhang, and K. Letaief, "Throughput and energy efficiency analysis of small cell networks with multi-antenna base stations," *IEEE Trans. Wireless Commun.*, vol. 13, no. 5, pp. 2505 – 2517, May 2014.
- [49] X. Li, E. Björnson, E. G. Larsson, S. Zhou, and J. Wang, "A multi-cell MMSE detector for massive MIMO systems and new large system analysis," in *Proc. IEEE Global Telecomm. Conf.* IEEE, Feb. 2015, pp. 1–6.
- [50] J. Jose, A. Ashikhmin, T. L. Marzetta, and S. Vishwanath, "Pilot contamination and precoding in multi-cell TDD systems," *IEEE Trans. Wireless Commun.*, vol. 10, no. 8, pp. 2640–2651, Jun. 2011.
- [51] I. Atzeni, J. Arnau, and M. Debbah, "Fractional pilot reuse in massive MIMO systems," in *Proc. IEEE Int. Conf. Commun.*, London, UK, Jun. 2015, pp. 1030–1035.
- [52] S. V. Hanly and D. N. C. Tse, "Resource pooling and effective bandwidths in CDMA networks with multiuser receivers and spatial diversity," *IEEE Trans. Inf. Theory*, vol. 47, no. 4, pp. 1328–1351, May 2001.
- [53] D. J. Daley and D. Vere-Jones, *An introduction to the theory of point processes: volume II: general theory and structure*. Springer Science & Business Media, 2007.